Analysis of scattered signal to estimate reservoir fracture parameters

Samantha Grandi K., Mark E. Willis, Daniel R. Burns and M. Nafi Toksöz
Earth Resources Laboratory
Dept. of Earth, Atmospheric, and Planetary Sciences
Massachusetts Institute of Technology
Cambridge, MA 02139

May, 2007

Abstract

We detect fracture corridors and determine their orientation and average spacing based on an analysis of seismic coda in the frequency-wave number (*f-k*) domain. Fracture corridors have dimensions similar to seismic wavelengths which causes scattering. The distribution of energy in shot records in the *f-k* domain depends upon the orientation of the records relative to the fracture strike. In the direction normal to fractures, scattered waves propagate with slower apparent velocities than waves propagating along the fracture channels. The associated *f-k* spectral differences allow the identification of the preferred fracture orientation and spacing. We apply our technique to a fractured reservoir in the Lynx field, in the Canadian foothills. The estimated preferential fracture orientation is about N40°E, which agrees with regional stress measurements. The average fracture spacing is 75 m on the West side of the survey, while fractures are more sparse on the East side. We also apply the Scattering Index methodology (Willis et al., 2006) to the same data, post-stack and pre-stack. This technique has higher resolution to map fracture distribution, intensity and orientation, and therefore complements the spectral method in providing an integrated description of reservoir fractures.

1 Introduction

The detection of reservoir fractures using seismic methods has been traditionally based on effective medium theories that assume fractures in a rock mass are much smaller than the wavelengths and their effects are distributed throughout the bulk. Fractures can also be modeled as discrete inclusions in the medium. The linear slip deformation theory (Schoenberg, 1980) is particularly fit to study the discrete effects of fractures as it expresses a single fracture as a displacement discontinuity, the magnitude of the displacement jump being related to the specific fracture stiffness. This theory predicts a frequency dependent seismic response and agrees with experimental observations of wave propagation through fractured rocks (Pyrak-Nolte et al., 1987).

Schoenberg's approach has also been used to model the complicated phenomena that occur in the presence of multiple parallel fracture sets including seismic scattering and wave guiding (e.g. Yi et al., 1997; Daley et al., 2002). By analyzing some of these types of fracture models, Willis et al. (2006), developed a novel and practical technique to characterize fractures at the reservoir level known as the Scattering Index method. Discrete approaches are valid in the limit where seismic wavelength is comparable to fracture dimensions. The seismic response of "fracture corridors" is characterized by scattered energy present in the coda of seismic waves which is usually considered noise in signal processing but contains valuable information about the fracture geometry and properties. For instance, the spacing between multiple parallel fractures introduces a characteristic length scale for the rock mass. When waves propagate perpendicular to a periodic set of fractures a stop-band behavior is produced (Grandi et al., 2005).

We analyze scattering energy from a field in the Canadian foothills in the frequency-wave number domain aiming to estimate the orientation and mean spacing of the fracture corridors.

2 *F-K* Analysis of Scattered Signal

Our methodology to detect the presence of fractures at the seismic scale, their preferential orientation and average spacing is derived from analyses of synthetic shot records of reservoirs containing regularly spaced vertical fractures.

Figure 1 shows synthetic shot gathers and their *f-k* spectra corresponding to a model of 5 horizontal layers in which the third one simulates a fracture corridor of 35 m spacing with stiffness of 4e9 Pa/m embedded in a typical reservoir rock. The numerical modeling is based on a finite difference approximation and the implementation of fractures follows Coates and Schoenberg (1995). The dimensions of the multiple fractures set are similar to the dominant wavelengths (λ) propagating across and along it; for this model in particular, fracture vertical length is about 2λ, horizontal length is about 10λ and spacing is about $\lambda/3$. The fracture channels are long enough to act as wave guides and the spacing between fractures is such that seismic waves are expected to scatter (Xian et al., 2001).

The record in the middle of figure 1 depicts data collected normal to fracture strike; the one on the right shows the behavior in the direction parallel to fractures and the left most one shows the no-fracture case. On the bottom row, 2D Fourier transforms are computed in a window in time and offset that includes the reservoir. Data windowing is necessary to isolate the main signal related to the fractured level from overlying formations, conversions observed at far offsets, direct arrivals, move out and mute effects.

All the arrivals corresponding to P-P reflections and some P-S conversions occurring at the main model interfaces are identifiable irrespective of the presence of fractures or the recording angle, however, fractures introduce significant energy affecting the coherence of the last two reflectors.

The spectral character of the scattered energy varies with azimuth:

1. Parallel to fracture strike, the time domain response includes numerous "multiple" reflections below the P-P reflector associated to the top of the reservoir. Since these events have similar move out (positive) to the primaries, they map in their vicinity on the *f-k* space.

2. Normal to fracture strike, the backscattered energy shows reverse linear move out in the time-offset space. In the *f-k* domain, this energy maps in the negative wave number plane which is key in our analysis. The forward scattered signal from the fractures maps into the positive wave number quadrant and is smeared out.

To determine fracture orientation, we compare the backscattered energy at different azimuths by summing the square of the amplitudes in the negative wave number quadrant (Grandi et al., 2005):

$$E_{scatt} = \sum_{-k_N}^{-k_o} A^2 \tag{1}$$

where k_N refers to the Nyquist wave number and k_o is chosen so that energy falling onto the $k = 0$ axis is not included in the sum. This value is in practice required to be greater than zero given the intrinsic resolution of the Fourier transform of band-limited signals. The backscattered energy in equation 1 is maximized when the orientation is perpendicular to fracture strike. Such behavior is consistent in all modeled cases where we have varied fracture spacing, vertical length and stiffness (figure 2a). Fractures' backscattered signal can be isolated by designing reject-pass filters in the *f-k* space.

An immediate advantage of analyzing fracture signals in the Fourier domain pertains to the determination of the nominal spacing between fractures. Fracture spacing (D) is measured from the data spectrum in the negative wave number plane in the direction normal to fractures by taking one-half of the inverse

of the dominant wave number (k) or, alternatively, estimating the characteristic apparent velocity of the backscattered events (V) and their dominant frequency (f):

$$D = \frac{1}{2}\frac{V}{f} = \frac{1}{2}\frac{1}{|k|} \tag{2}$$

A similar relationship between fracture spacing and frequency was observed by Rao et al. (2005), who analyzed the spectral notches of transfer functions extracted from azimuthal stacks.

Backscattered signal exhibits lower frequency-wave number when the spacing is larger whereas fracture vertical length or stiffness have little effect on the spectral components (figure 2b). Peak frequency also decreases as the window of analysis is extended or shifted in time, but peak wave number remains constant.

Models with different fracture stiffness show that the more compliant the fractures are the more the fracture signals interfere with the reflections and conversions from the interfaces. An increase of fracture stiffness of about 1 order of magnitude decreases spectral amplitudes of backscattered waves by about 30° (figure 2c). Similarly, shortening the vertical length of the fractures (the thickness of the fractured bed) causes backscattered amplitudes to drop (figure 2d).

The analysis of modeled data suggests that fracture stiffness, vertical length and spacing affect the amplitude of backscattered waves, however fracture spacing solely defines their dominant wave number component. The effects of fractures on the seismic spectral response are azimuthally dependent and stronger in the fracture normal direction where properties can be conveniently estimated.

3 The Lynx Field Data

The Lynx field is located in southwest Canada, on the foothills of the Canadian Rocky Mountains. Gas production in Lynx is largely controlled by fractures at the main reservoir unit, (Cadotte Formation), which is a tight-gas sandstone at a depth of about 3.4 Km. Successful well placement relative to the structure is complicated by the fact that the reservoir thickness for most of the area is below seismic resolution. In addition, tectonics in the region has extensively folded the southwest section around the reservoir level, with the major axis of these folds being in the NW-SE direction. In the eastern part of the survey, the structural folding is reduced and flattens smoothly into a vast plain. Evidence of fractures in the Cadotte comes from outcrops, core analyses, resistivity, and image logs in several wells. Seismic data used in our analysis correspond to an area approximately 1.5 Km away from the location of most of these wells. Breakouts are observed in many wells indicating that the horizontal stresses are unequal in this region. The orientation of SHmax, inferred from well breakouts and tensional fractures, is consistent at NE-SW (figure 3).

Great care was taken to ensure that the scattered signals were preserved throughout preprocessing. In particular, we worked with VeritasDGC to preserve the near offsets and angular fold by limiting bin flexing and trace mixing processes. Input data for our analysis were non-migrated. To avoid possible acquisition footprint issues, the data were sorted into 20° azimuthal groups with an overlap of 10 degrees, and the analysis was carried out only in gathers where full azimuthal fold was found. Offset distribution in each azimuthal gather was checked for homogeneity.

The reservoir P-wave velocity varies widely across the area, from around 4500 m/s to 6300 m/s. The seismic frequency bandwidth at the reservoir level ranges between 20 and 50 Hz, which implies that dominant wavelengths are greater than 90 m. The receiver spacing was 60 m.

4 F-K Method on the Lynx Field

Azimuthal *f-k* transforms are computed for shot records of Lynx's survey that have acceptable fold. The analysis is performed in a time window of about 0.45 s starting at the horizon corresponding to the top of Cadotte (figure 4). Offsets are limited between 400 and 3000 m.

Following the procedure for determining fracture orientation, we estimate the backscattered energy to be the sum of the amplitudes squared in the negative wave number quadrant and compare among azimuths.

As previously explained, we expect that the amount of backscattered energy is maximized when data are collected perpendicularly to fracture strike. As an example, figure 5 depicts the variation of the backscattered normalized energy at each angle for two particular shot points whose locations are shown on figure 3. In shot 34125 the energy function peaks at 140° and 300-320° (which are 180° away). In shot 30136 a clear maximum is reached at 300°. These azimuths indicate the direction normal to fractures at these locations.

In the same figure, the *f-k* spectra of the azimuthal components at the normal and parallel direction are shown. As predicted by the models, energy is less distributed in the *f-k* space in the direction of fractures. The *f-k* spectrum of the normal component of shot 34125 exhibits an energy maximum in the negative wave number at about 32 Hz and -0.008 1/m, hence the estimated fracture spacing is approximately 62 m at this location. At the location of shot 30136 fracture spacing increases to about 164 m.

Figure 6 shows a map of orientation and spacing of fractures found at the Cadotte level. Fracture spacing is relatively regular across the western part of the survey, varying between 60 m and 120 m approximately. On the East part, fractures of seismic scale seem to become more sparse or non existent. This interpretation is consistent with the structural behavior of Cadotte.

5 Scattering Index Analysis

Another way of processing scattered signals to derive fracture properties is described in Willis et al. (2006). These authors developed a method, called the Scattering Index (*SI*), to estimate reservoir fracture distribution and orientation. The method provides maps at the reservoir level of scattered energy associated with the presence of fracture corridors.

In the *SI* method, azimuthal transfer functions of the fractured zone are obtained by deconvolving a wavelet computed from above the reservoir from a wavelet computed from below. Transfer functions are less temporally compact in the direction parallel to fractures. The scattering index is a number that measures how much energy the transfer function has at non-zero lag values. When compared azimuthally, the largest *SI* value renders the direction of fractures.

The Scattering Index method is performed in the CDP domain as opposed to the *F-K* method which is applied in the SHOT domain. Another practical difference between the methods is the length of the time window of analysis. In the *SI* method the analysis is performed locally, around the horizon of interest, whereas in the *F-K* method the input data consist of the relatively long coda found after the reflector associated to the top of the reservoir (figure 4). Unlike the *F-K* method, the *SI* method is intrinsically insensitive to overprinting since it looks for differences in the wavelet as a function of depth, as it crosses the reservoir.

Figure 7 shows the pre-stack scattering index results. Fracture orientation is depicted in colors. Areas of intensive fracturing tend to align with the main structural trends and in these areas fractures are mostly oriented N-S and NE-SW as the regional maximum stress. In figure 8, where fracture orientations are represented with vectors, the local variations are more easily appreciated. The information is superimposed to the Cadotte time topography along with faults interpreted from migrated sections (provided by Conoco-Phillips). Cadotte's weak reflectivity and reservoir thickness (below seismic resolution) make the interpretation of faults and the mapping of structures with higher definition difficult. The bands of intense fracturing mapped with the *SI* method could be used as a guide to interpret faults and locate new wells.

In order to compare these results with those of the *F-K* method, an upscaled histogrammed version of the pre-stack *SI* analysis is shown in figure 9 as rose diagrams to match the measurement resolution of the *f-k* analyses. Orientations estimated from both methods agree for most of the area.

We apply the scattering index concept for the first time on post-stack as an initial and quick evaluation of the "intensity" of fracturing in an interval of interest. Once the data are stacked the azimuth information is lost and the method can only indicate the relative amount of scattering from one CDP location to the next. For instance, the map in figure 10 shows normalized scattering indices at the Cadotte level computed post-stack. Black areas correspond to highest values of *SI* and possibly to areas of more intense fracturing, areas in which fractures are more tuned to seismic wavelengths and/or areas where fractures are more compliant. A strong correlation is observed between this map and the pre-stack result of figure 7. The post-stack

scattering index map and vector lengths in the map of figure 8 indicate the intensity of scattering which might be related to fracture compliance or thickness variations of the reservoir.

6 Conclusions

We apply two methods to describe fracture corridors in a reservoir. In general, fracture orientations obtained from the Scattering Index method and our *F-K* analysis technique agree quite well across the survey. The dominant fracture direction coincides with the regional maximum horizontal stress orientation (NE-SW). The *SI* method provides a higher resolution map showing local variations in fracture orientations. The spectral method complements the fracture description by providing an estimation of fracture spacing. We have found that relative fracture stiffness might be extracted from the scattered waves' amplitudes if reservoir thickness is known, but a quantitative estimation would require a better understanding of attenuation phenomena in fractured media. In Lynx, our results provide additional, more detailed information about the reservoir to aid in its seismic interpretation.

7 Acknowledgements

The authors would like to thank: Tad Smith and Kent Milani from VeritasDGC for providing the field data tailored to our needs; and Doug Foster, Dave Lane, Ethan Nowak and Dean Sinnott from Conoco-Phillips for valuable discussions and technical information. This work has been supported by the Founding Member Consortium of the Earth Resources Laboratory at MIT and DOE award number DE-FC26-06NT42956.

References

Coates, R. and Schoenberg, M. (1995). Finite-difference modeling of faults and fractures. *Geophysics*, 60(5):1514–1526.

Daley, T., Nihei, K., Myer, L., Majer, E., Queen, J., and Murphy, J. (2002). Numerical modeling of scattering from discrete fracture zones in a San Juan basin gas reservoir. In *Expanded Abstracts*. Society of Exploration Geophysicists, 70th Annual International Meeting.

Grandi, S., Willis, M. E., Burns, D. R., and Toksöz, M. N. (2005). F-K analysis of backscattered signal to estimate fracture orientation and spacing. In *Annual Report*. Borehole Acoustics and Logging and Reservoir Delineation Consortia, Earth Resources Laboratory, MIT.

Pyrak-Nolte, L., Cook, N., and Myer, L. (1987). Seismic visibility of fractures. In *28th US Symposium on Rock Mechanics*, pages 47–56.

Rao, R., Willis, M., Burns, D., Toksöz, N., and Vetri, L. (2005). Fracture spacing and orientation estimation from spectral analyses of azimuth stacks. In *Expanded Abstracts*, pages 1409–1412. Society of Exploration Geophysicists, 73rd Annual International Meeting.

Schoenberg, M. (1980). Elastic wave behavior across linear slip interfaces. *Jounal of the Acoustical Society of America*, 68(5):1516–1521.

Willis, M., Burns, D., Rao, R., Minsley, B., Toksöz, N., and Vetri, L. (2006). Spatial orientation and distribution of reservoir fractures from scattered seismic energy. *Geophysics*.

Xian, C., Nolte, D., and Pyrak-Nolte, L. (2001). Compressional waves guided between parallel fractures. *International Journal of Rock Mechanics and Mining Sciences*, 38:765–776.

Yi, W., Nakagawa, S., Nihei, K., Rector, J., Myer, L., and Cook, N. (1997). Numerical investigation of fracture-induced seismic anisotropy. In *Expanded Abstracts*. Society of Exploration Geophysicists, 67th Annual International Meeting.

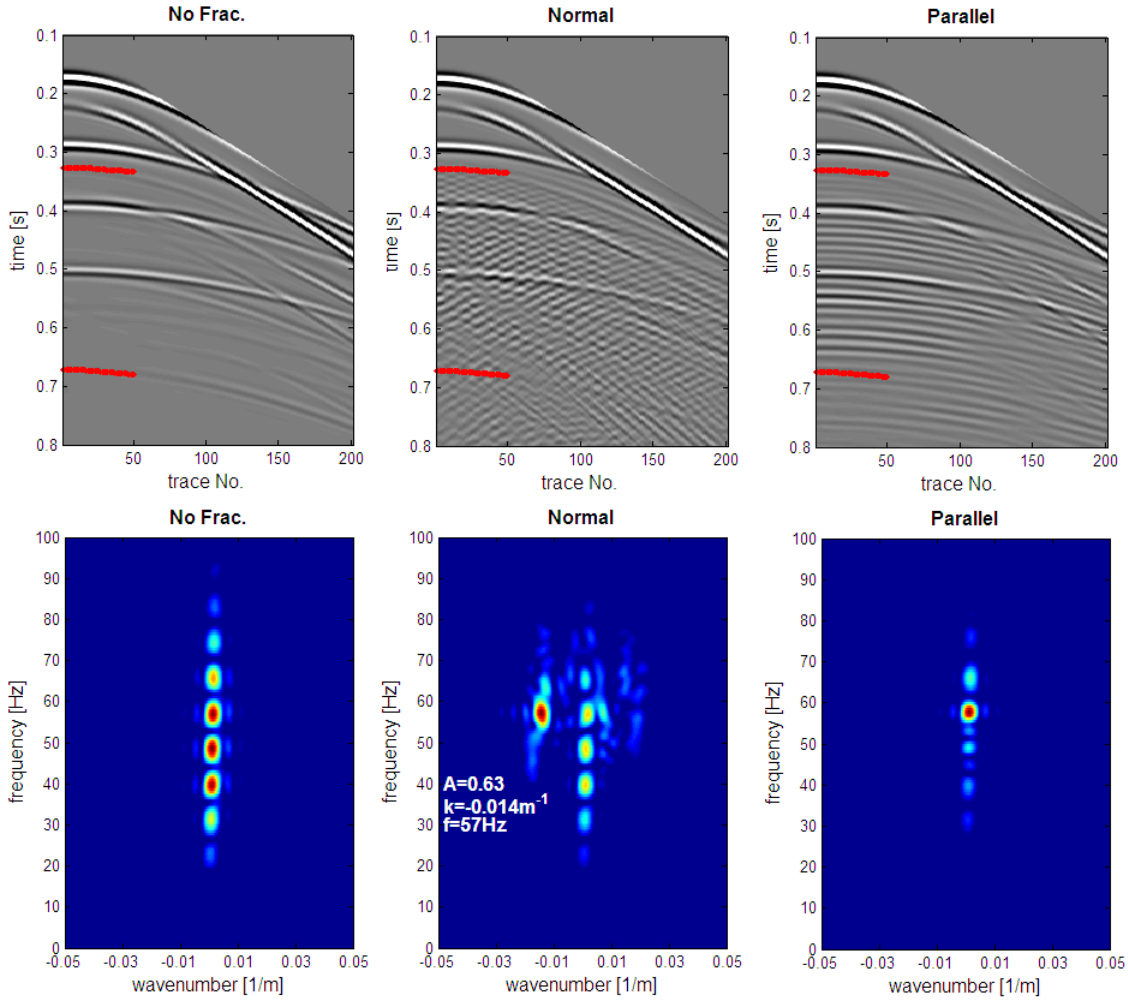

Figure 1: Spectral analysis of modeled data. At the top row shot records collected in the normal (middle) and parallel to fracture orientation (right) for a model of 5 layers with fractures in the 3rd. layer separated 35 m. Fracture stiffness is 4e9 Pa/m. *F-k* spectra are shown at the bottom row. Fractures induce strong scattering not present in the equivalent no-fracture model on the left column. In the normal direction, the -0.014 1/m, 57 Hz component has maximum energy. Equation 2 yields a fracture spacing of 35.7 m.

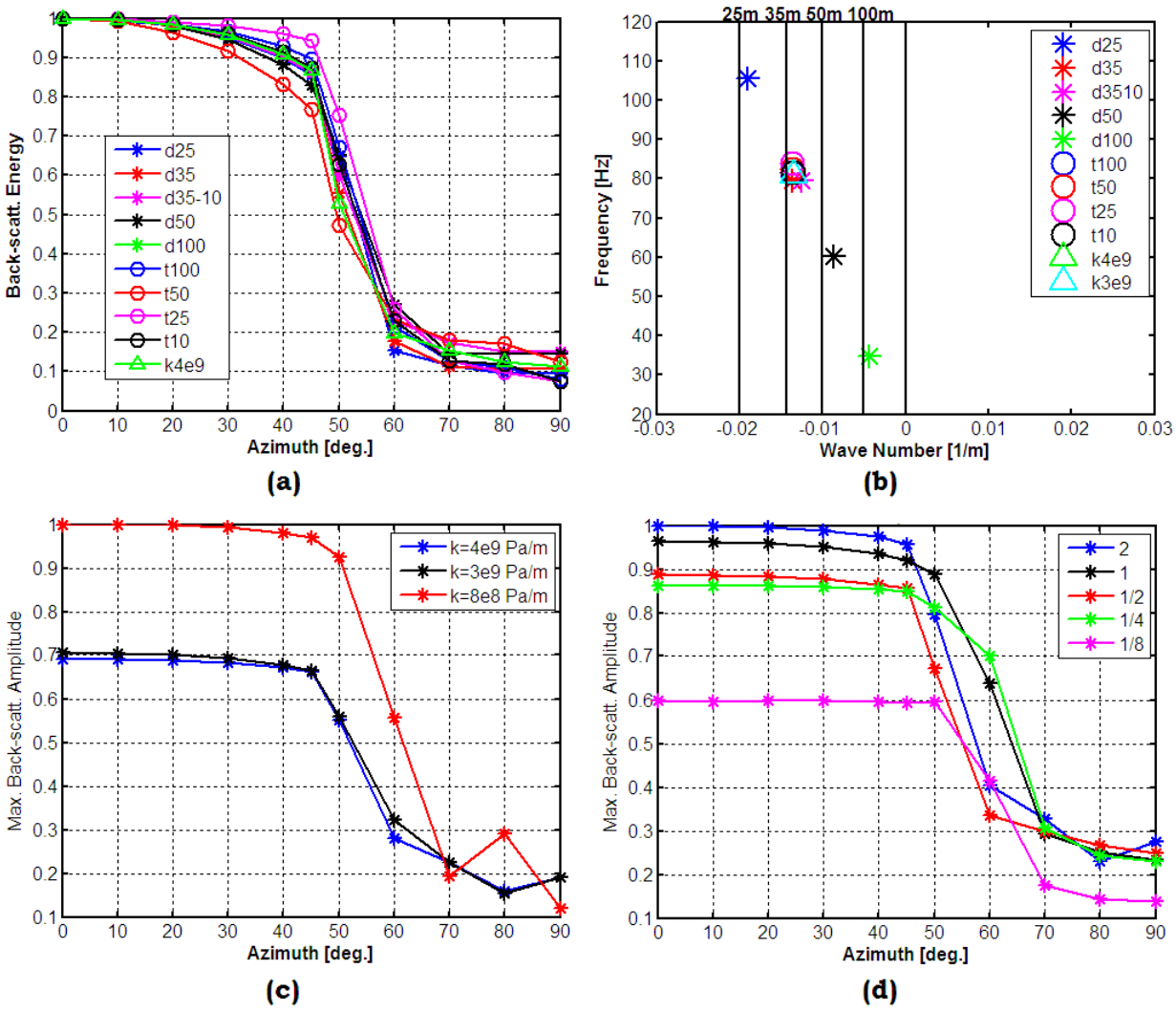

Figure 2: Backscattered energy as a function of azimuth for all models (a). At 0° (the direction normal to fractures) peak wave number is related to fracture spacing (b). In the labels "d" indicates fracture spacing (in meters); "t" thickness of fractured bed (in meters) and "k" fracture stiffness (in Pa/m). Unless it is indicated fracture spacing is 35 m, fracture stiffness is 8e8 Pa/m and thickness of the bed is 200 m (2λ). Figure (c) and (d) show the decrease of back-scattered waves amplitudes when the compliance and the thickness of the fractured bed are reduced, respectively. In figure (d), thickness is labeled in terms of P-wavelength.

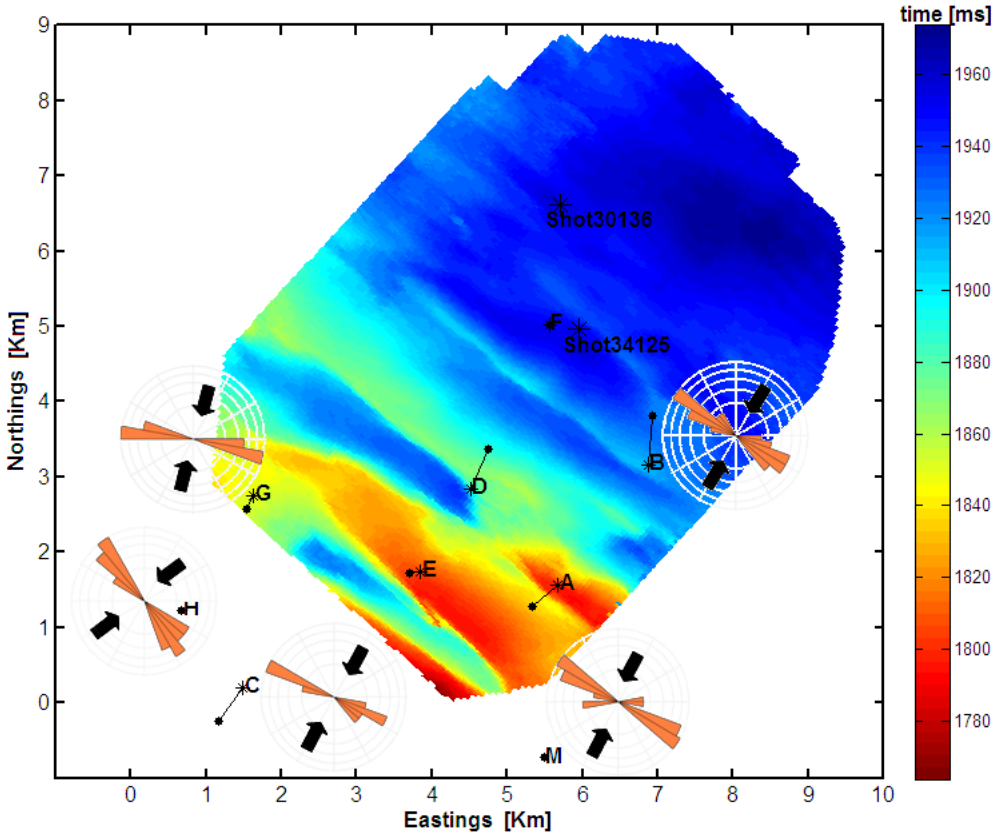

Figure 3: Survey area. In colors, Cadotte time map. Well locations are indicated with capital letters. Direction of well breakouts (orange) and the orientation of SHmax (black arrows) are superimposed.

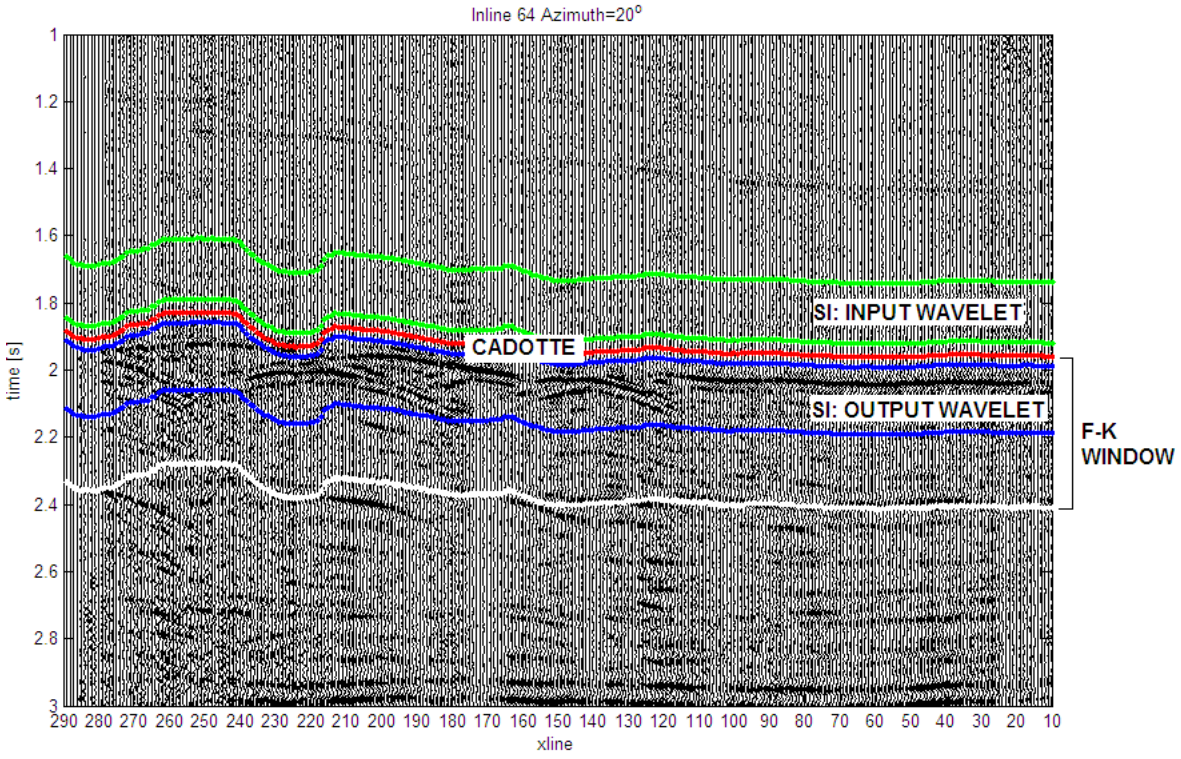

Figure 4: Windows of data input in the fracture analysis. The horizon corresponding to the top of Cadotte is shown in red over a seismic section of Lynx. In the *F-K* method, spectral analysis is focused on the window spanning from Cadotte up to the time indicated in white. In the *SI* method, input and output wavelets are computed in short windows above and below the horizon.

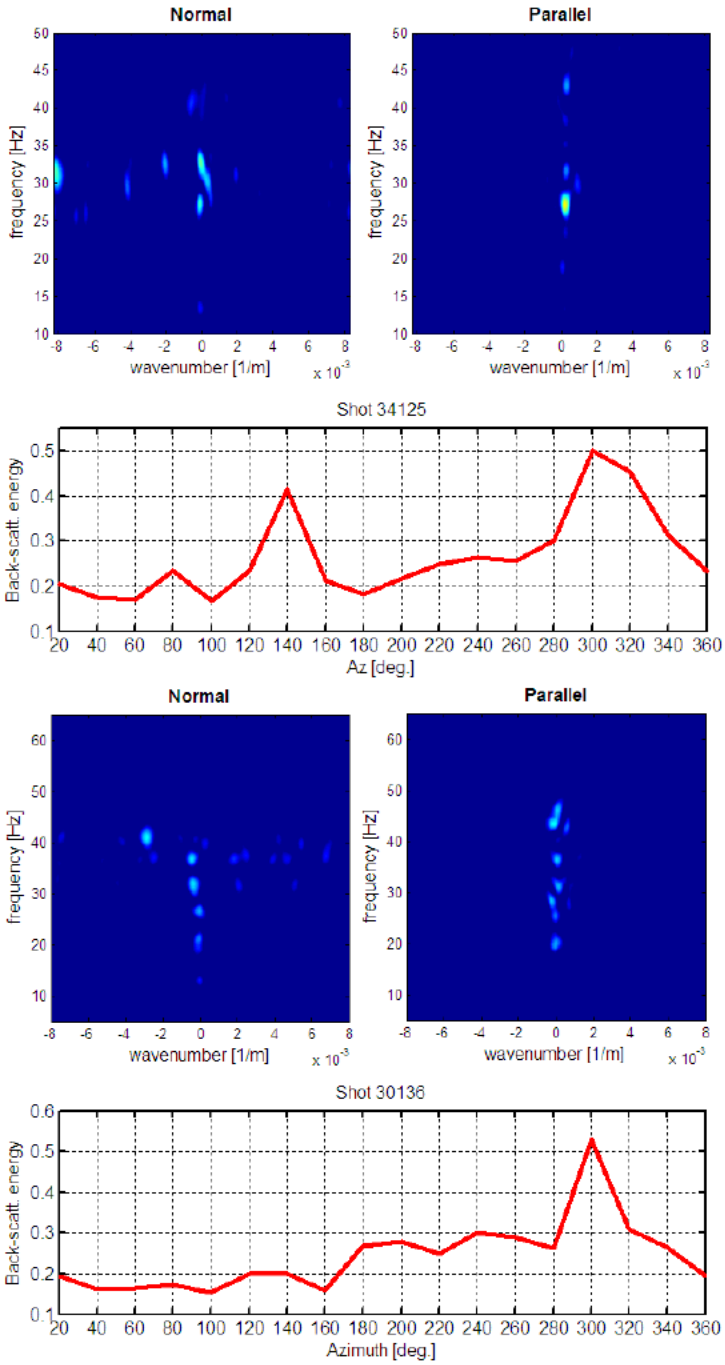

Figure 5: Examples of *f-k* analysis of two shots records. Shot locations are indicated in figure 3. Top rows show *f-k* spectra of data normal and parallel to fractures in shots 34125 (top) and 30136 (bottom). The graphs below depict the variation of backscattered energy with azimuth.

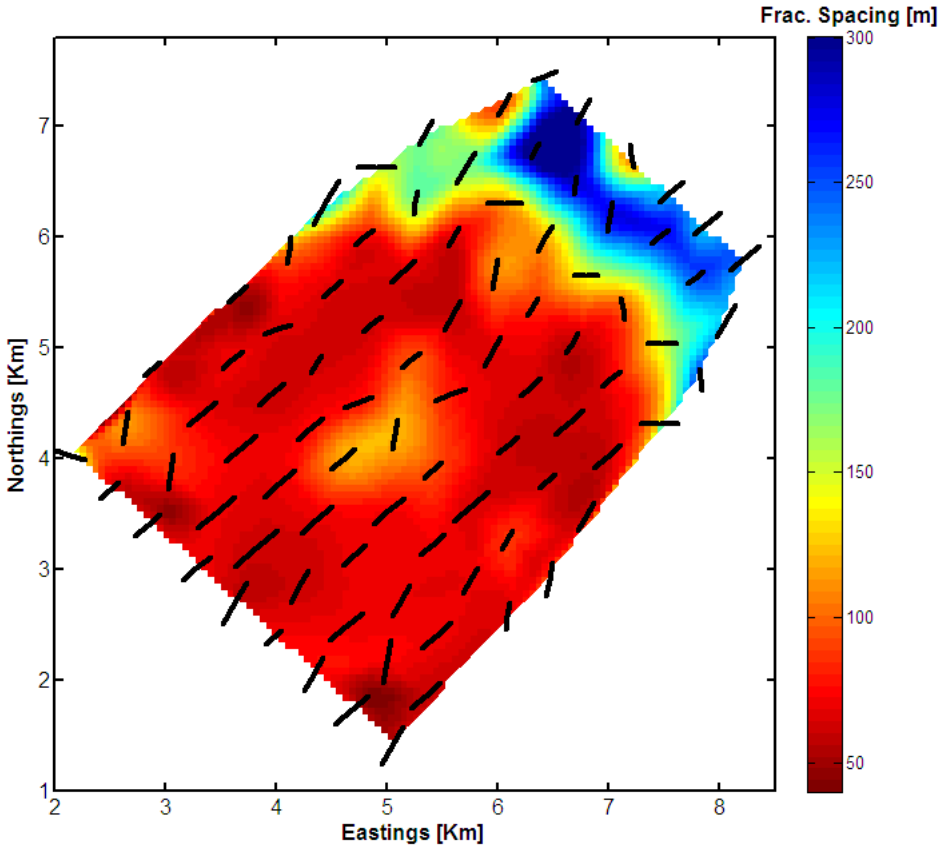

Figure 6: Fracture spacing map (color values are in meters) and fracture orientations (black quivers) obtained with the F-K method.

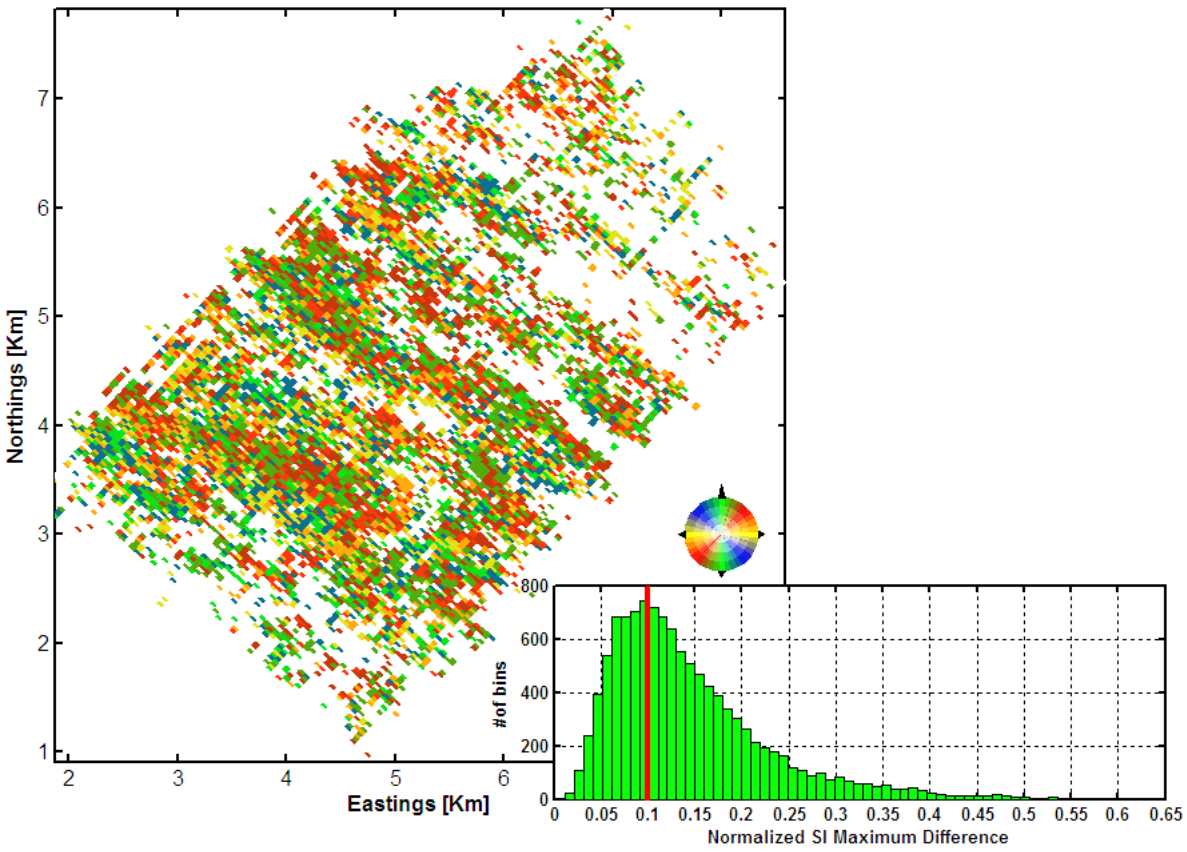

Figure 7: Map of *SI* pre-stack. Red line in the inset indicates level of threshold. The pre-stack result includes information about distribution, intensity and orientation of fractures depicted with colors.

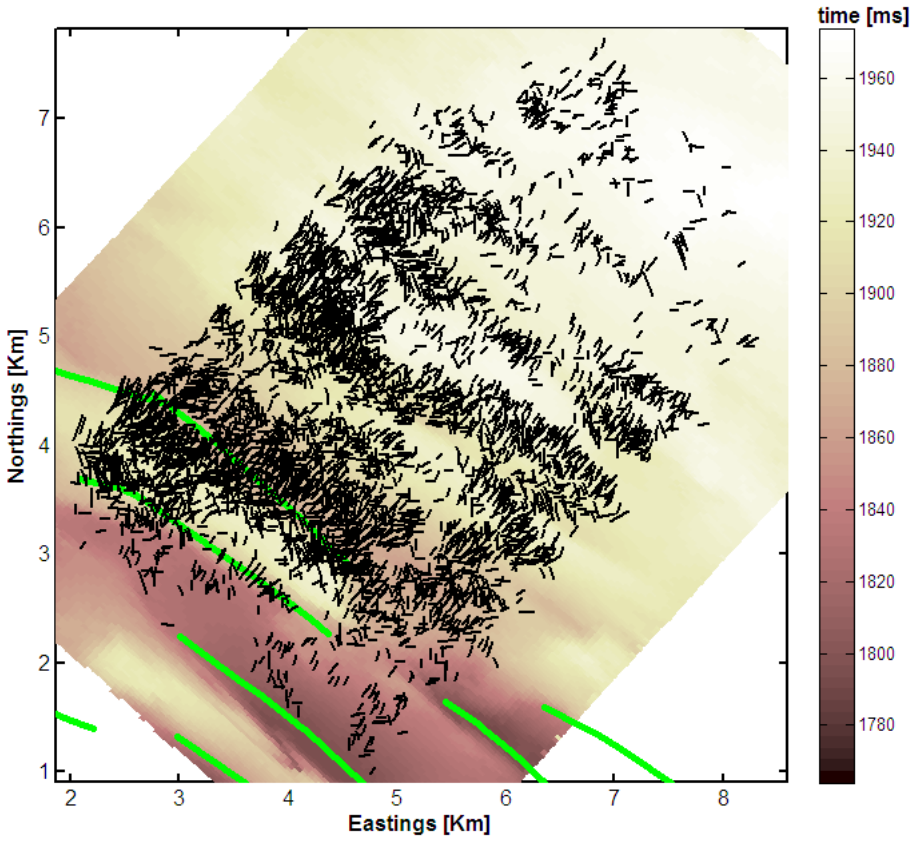

Figure 8: Map of fracture distribution, intensity (vector lengths) and orientation from the *SI* method. Quivers are plotted over Cadotte's time topography and traces of faults interpreted.

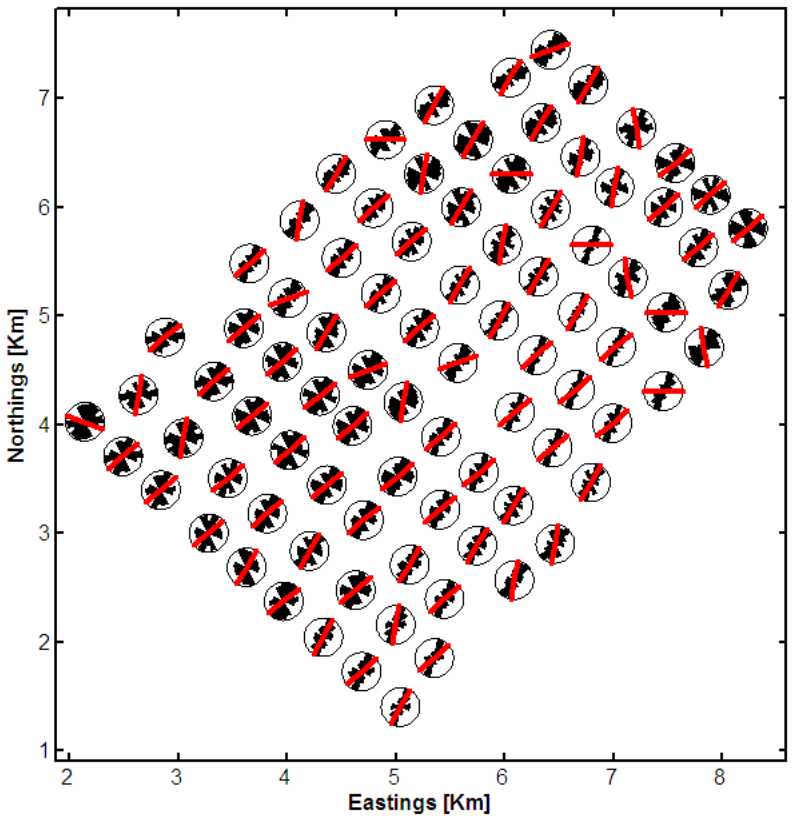

Figure 9: Map of fracture orientations at the reservoir obtained with the F-K method (red quivers) and with the SI method (black rose diagrams)

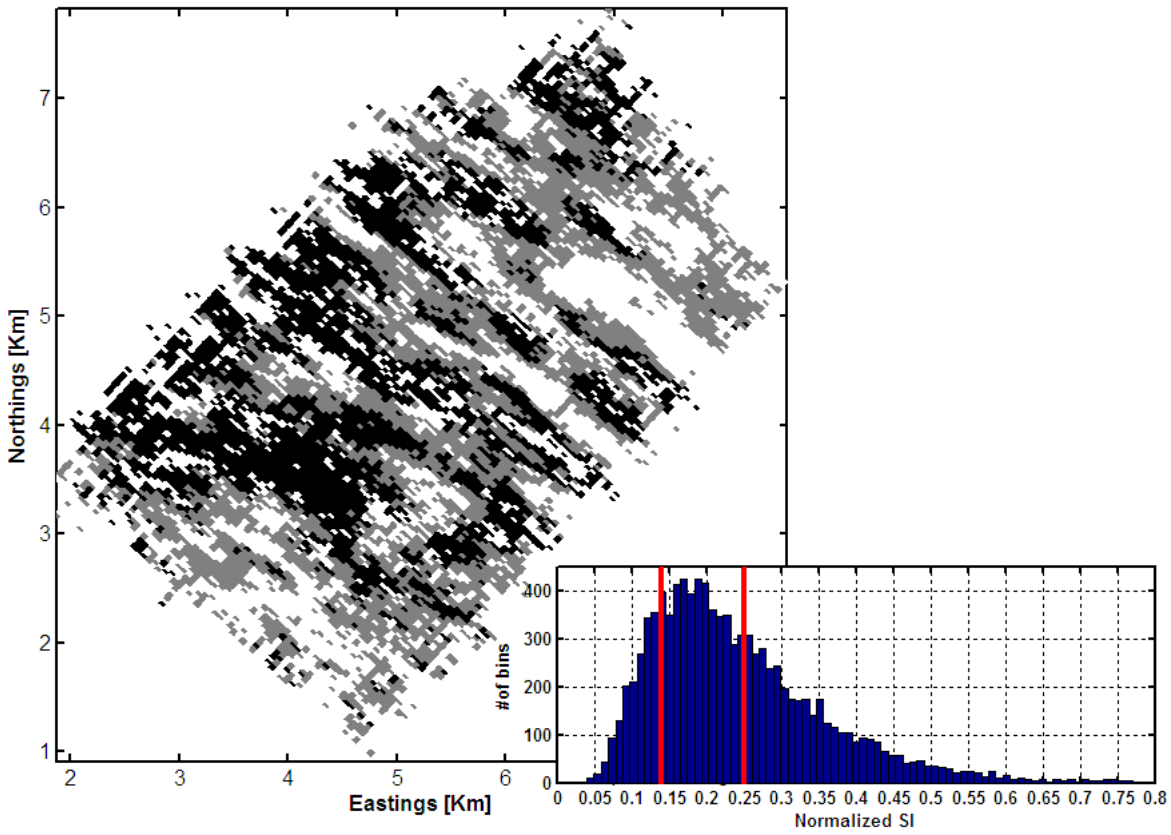

Figure 10: Map of *SI* post-stack. Red lines in the inset indicate levels of threshold.